JOINT INVERSION OF CRUSTAL AND UPPERMOST MANTLE STRUCTURE IN WESTERN CHINA

Xiaodong Song[1], Zhen Xu[1], Lupei Zhu[2], and Yuming Zhou[2]

University of Illinois at Urbana-Champaign[1] and Saint Louis University[2]

Sponsored by the Air Force Research Laboratory

Award No. FA9453-10-C-0216
Proposal No. BAA10-55

ABSTRACT

In seismic inversion, trade-offs between model parameters are well known. To resolve the ambiguity and to improve resolution, a combination of different datasets that have sensitivities to different parameters is required, or a priori constraints have to be imposed. The objective of this research is to develop joint-inversion methods involving P travel times (including secondary P), receiver functions, and surface-wave dispersion measurements from ambient noise correlation and apply them to the western China region to obtain 3D models of P and S structures of the crust and upper mantle.

Our joint inversions are done in two steps. First, we jointly invert P travel-time datasets that include first-arriving Pg and Pn and secondary crustal direct P waves. This gives us a 3D model of crustal Vp, a Pn velocity map, a Moho depth map, and Pn station delays. Inclusion of secondary crustal direct P waves improves the resolution of lower crust, and the joint inversion allows the separation of crustal velocities and Moho depth variation. Second, we combine the P model and Pn station delays from the first step with receiver functions and Rayleigh-wave dispersion measurements to invert jointly for S wave structure and Moho depth. Adding well-constrained P model and Pn station delays will help the joint inversion of receiver functions and surface-wave dispersions to find the right S model when the crustal Vp/Vs ratio is not known, which is often the case.

This is the first year of the project. We report progress made on the following two areas: (1) development of joint-inversion methods and (2) new dispersion measurements and dispersion maps from a combination of both ambient noise data.

OBJECTIVES

The objective of this research is to develop joint-inversion methods involving P travel times, receiver functions, and surface-wave dispersion measurements from ambient noise correlation and to apply them to the western China region to obtain 3D models of P and S structures of the crust and upper mantle.

RESEARCH ACCOMPLISHED

Join Inversion Methods

Trade-offs between model parameters are well known in seismic inversions. To resolve the ambiguity and to improve resolution, a combination of different datasets that have sensitivities to different parameters is required, or a priori constraints have to be imposed. For example, it has long been recognized that the teleseismic P receiver functions are primarily sensitive to shear-wave velocity (Vs) contrasts and depth-velocity product and not the velocity alone (Ammon et al., 1990). On the other hand, surface waves are primarily sensitive to the vertical shear-velocity averages. Thus, joint inversion (or analysis) of receiver functions and surface-wave dispersions has now been commonly used to resolve depth resolution of Vs structure (e.g., Julia et al. 2000; Ozalaybey et al., 1997). Similarly, crustal thickness estimated using only the delay time of Moho P-to-S converted phase (Ps) relative to P at the receiver trades off strongly with crustal Vp/Vs ratio, which can be remedied using later converted phases (Zhu and Kanamori, 2000).

Our joint inversions are done in two steps. First, we jointly invert our P travel-time datasets, including first-arriving Pg and Pn, and secondary crustal direct P. This gives us a 3D model of crustal Vp, a 2D Pn velocity map, a Moho depth map, and Pn station delays. Second, we combine the P model and Pn station delays from the first step with receiver functions and Rayleigh-wave dispersions to invert jointly for S wave structure and Moho depth.

Step 1. Joint inversion of Pg, Pn, and secondary crustal P for crustal P velocities, Moho depths, and Pn velocities

We have recently designed an iterative scheme to invert jointly for the velocities of the whole crust and the Pn waves as well as the Moho depth and have found it to be highly effective (Xu and Song, 2009). The method uses crustal Pg waves, head waves Pn, and secondary direct P waves at distances greater than the Pn and Pg crossover distance. These secondary arrivals are often very energetic and are quite abundant in earthquake bulletins (Figure 1). The advantage of a joint inversion approach is several-fold. First, Pn waves and secondary P waves at distances greater than the crossover distance provide constraint on crustal velocity in the lower crust. Second, with the resolution of 3D P velocity structure of the whole crust, Moho depth variation can be separately parameterized and simultaneously solved in the inversion. Third, with improved determination of Moho depth, different types of P waves can be better separated in the inversion iterations, thus reducing the contamination of P waves in the crust from Pn waves.

The joint inversion is a highly iterative. The gist includes rejecting bad data and sorting out different phases (Pg, Pn, secondary crustal P), effective ray tracing, formulating joint inversion of velocities and Moho, iterative selection of data with the improved models, and treatments on the inversion process (derivation of 1D model, parameterization, regularization and smoothing, and minimizer and linear-system solver). We use a spherical-coordinate 3D ray tracer that is based on a modification of the pseudo-bending ray (PBR) tracing method proposed by Koketsu and Sekine (1998). The joint inversions are formulated as follows:

Residual for Pg wave traveling from event j to station k can be approximated in the following linear form

$$r_{jk} = T_{jk}^{obs} - T_{jk}^{pred} = \sum_n \left(-\frac{dl}{v} \right) \left(\frac{\Delta v}{v} \right). \quad (1)$$

Residual for Pn wave traveling from event j to station k can be approximated as

$$r_{jk} = T_{jk}^{obs} - T_{jk}^{pred} = \sum_{n1}\left(-\frac{dl}{v}\right)\left(\frac{\Delta v}{v}\right)_m + \sum_{n2}\left(-\frac{dl}{v}\right)\left(\frac{\Delta v}{v}\right)_r + \eta\Delta h_k + \Delta t_j, \quad (2)$$

where the first the term on the right-hand side is the mantle contribution, and the second term is the contribution of velocity perturbation in the crust of the receiver side. The third term is the contribution of Moho depth variation at the receiver side. The combination of the 2nd and 3rd terms represents the station delay as in Equation 1. The last term is the event delay representing the uncertainty of event location, origin time, and Moho depth variation at the source side.

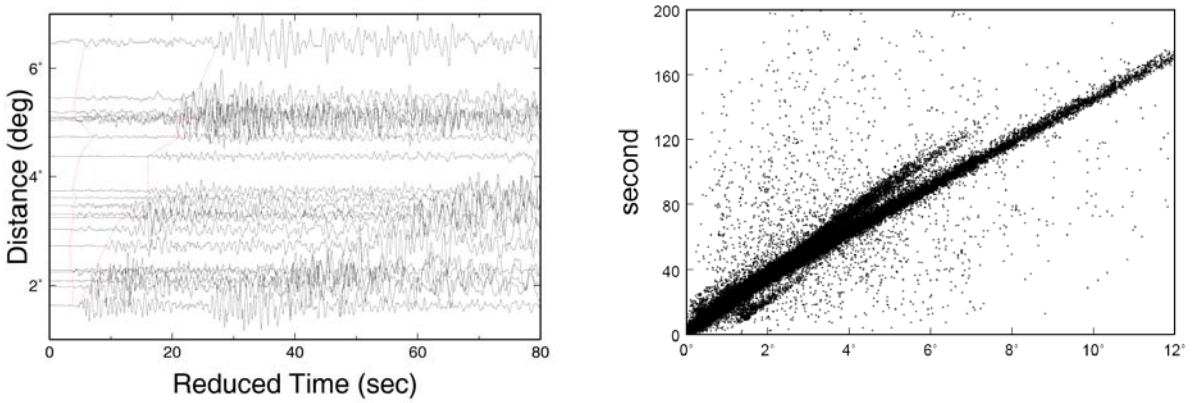

Figure 1. (Left) Example seismograms from Sichuan and Yunnan stations at regional distances. The travel time is reduced by 8 km/s. The lines show our travel-time picks. The nearly vertical line indicates first-arriving Pn waves. The second line indicates clear and strong secondary arrivals. The slowness is about 6.0 km/s. They are direct P waves turning at mid to lower crust. (Right) Raw travel-time picks from stations at Sichuan and Yunnan region. Data are from the Annual Bulletins of Chinese Earthquakes and Sichuan and Yunnan provincial earthquake bulletins. Note clear secondary arrivals, after Pn, at distances from 4 to 7 degrees.

Step 2. Joint inversion of receiver functions, surface wave dispersions, and Pn station delay for S velocities and Moho

The combination of receiver functions and surface-wave dispersions bridges some resolution gaps associated with each individual dataset (e.g., Julia et al. 2000; Ozalaybey et al., 1997). Figure 2 shows an example of joint inversion of receiver function and surface-wave dispersions at an INDEPTH station.

However, important ambiguity remains. In the P receiver function, the Moho P-to-S converted phase (Ps) is generally the strongest. The Moho depth determined from the Ps delay (relative to P) trades off strongly with crustal Vp/Vs ratio. Multiple converted phases would help resolve the ambiguity (Zhu and Kanamori, 2000), but they are usually more difficult to identify. Sensitivity tests (Figures 3–4) suggest that adding well-constrained P information will help the joint inversion of receiver function and surface-wave dispersion to find the right S model when the Vp/Vs ratio is not known, which is often the case. Two types of P information from Step 1 can be used in the joint inversion of receiver functions and surface waves for S structure. One is to use directly the crustal P velocities under the station derived from the 3D P model. Another type of P information is the Pn station delay time, which provides a constraint on Moho depth and average crustal velocity.

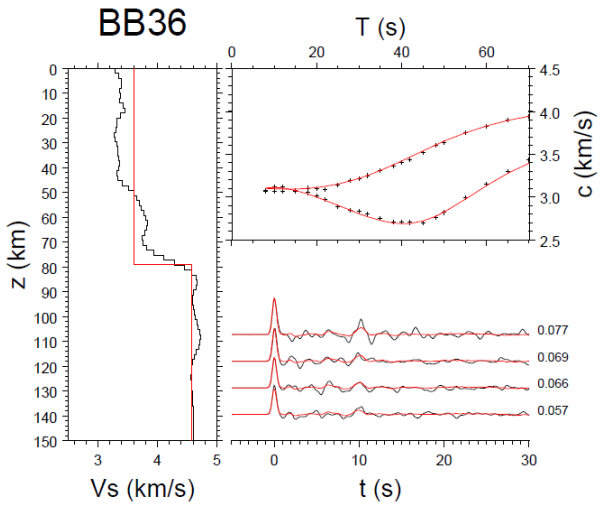

Figure 2. An example of joint inversion of receiver function and surface-wave dispersions. The left panel shows the S velocity model (black lines) from the inversion and the H-k stacking result (red lines). The right panel shows receiver function and surface-wave dispersion fits, black representing data and red representing prediction from the obtained S velocity model. The Vp/Vs ratios are fixed using the values obtained from the H-k stacking results.

A. Vp is known. **B**. Wrong Vp/Vs

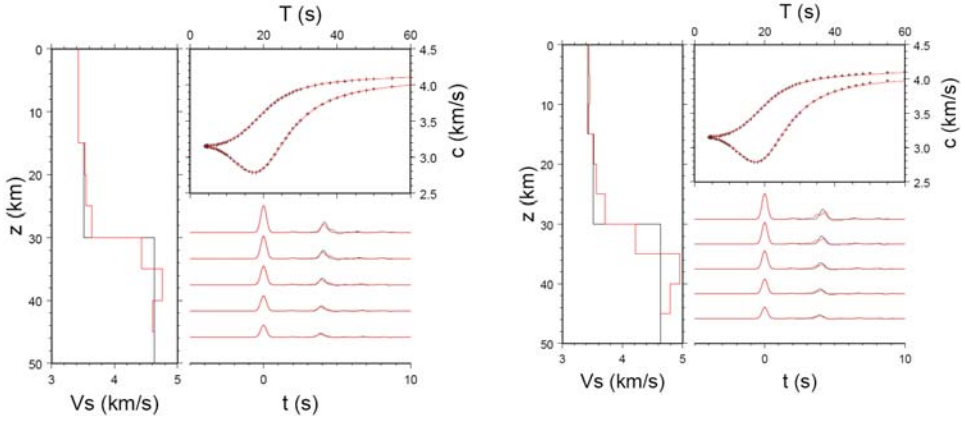

Figure 3. Tests on joint inversion of receiver functions and surface-wave dispersions, with and without prior knowledge of Vp structure. (A) Vp is set to the true values. Inverted Vs (red) matches the input model (black) relatively well. (B) Vp/Vs ratio is set to 1.7 (compared with the average 1.8 of the input model). Inverted Vs does not match the input as well as in (A), while the fits to dispersions (upper right) and receiver functions (lower right) are similar.

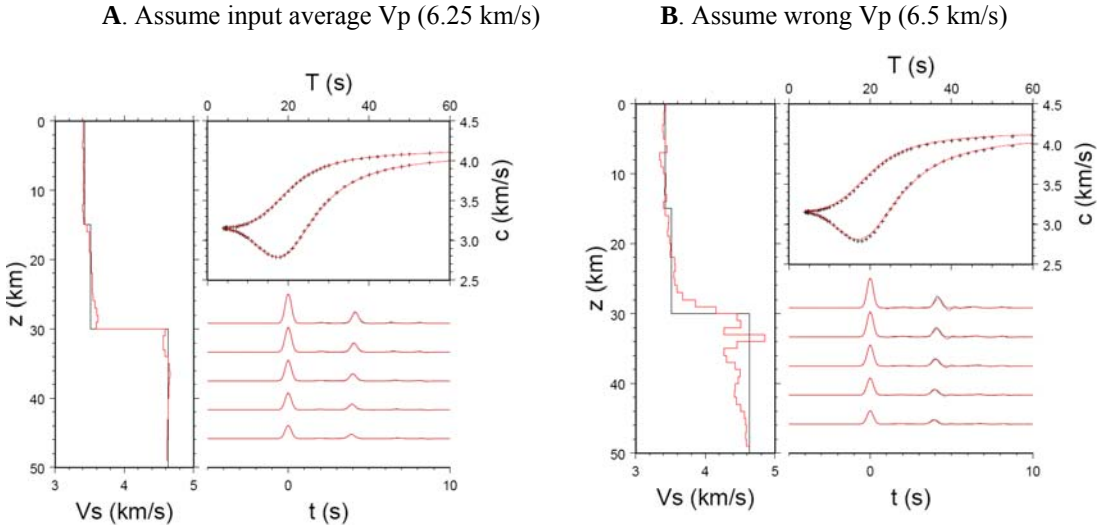

Figure 4. Synthetic tests on combining Pn station delay with receiver functions and surface-wave dispersion for a joint inversion. The input model is listed in Table 1. (A) Correct average crustal Vp (6.25 km/s) is assumed, which would yield the correct Moho depth (30 km) from Pn station delay. (B) Average crust Vp is assumed to be a wrong value of 6.5 km/s, yielding Moho depth of 33.3 km from Pn station delay. The S structure recovered in B is considerably poorer than in A and has a Moho (slightly less than 30 km) inconsistent with the Pn Moho (33.3 km).

New Dispersion Measurements and Dispersion Maps

Over the last few years, we have been working on ambient noise tomography of China (Zheng et al., 2008; Song et al., 2009). Recently, we have made a major effort to increase dispersion measurements by including stations over a long period of time and by including traditional earthquake data (Figure 5). For empirical Green's functions (EGFs), we have a total of 528 stations. The data are from 18 months of continuous data from the Chinese National Seismic Network (CNSN) (48 stations) and all the continuous broadband and long-period data in our study region available from 1991 to 2007 from permanent global and regional network stations as well as temporary Program for the Array Seismic Studies of the Continental Lithosphere (PASSCAL) stations from the Incorporated Research Institutions for Seismology Data Management Center (IRIS DMC). The earthquake data include events for all the stations from 155 earthquakes in our study region with depth shallower than 40 km and magnitude larger than 5.5 from 2000 to 2007. We also included event data recorded by CNSN stations for another 197 earthquakes with magnitude from 5.0 to 5.5 in the same depth range and time period.

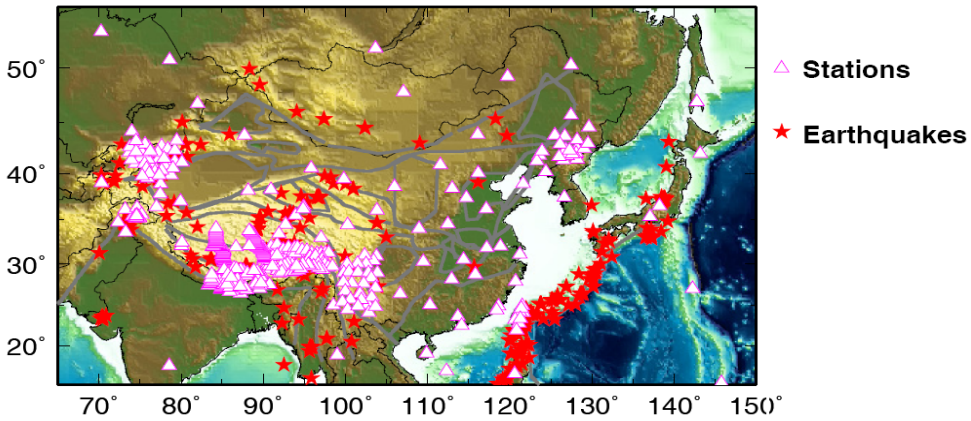

Figure 5. Distributions of stations (triangles) and earthquakes (stars) used in our study.

The EGFs are obtained using procedures from Bensen et al. (2007) and both group- and phase-velocity dispersion curves are measured from the EGFs using a frequency-time analysis (Levshin and Ritzwoller, 2001). For earthquake data, only group-velocity dispersion curves of earthquake data are measured in the same way. The new dataset has a maximum of ~35000 measurements for group velocity and ~22500 measurements for phase velocity at s period of 20 s (Figure. 6). We increase our total number of measurements by four times in this process.

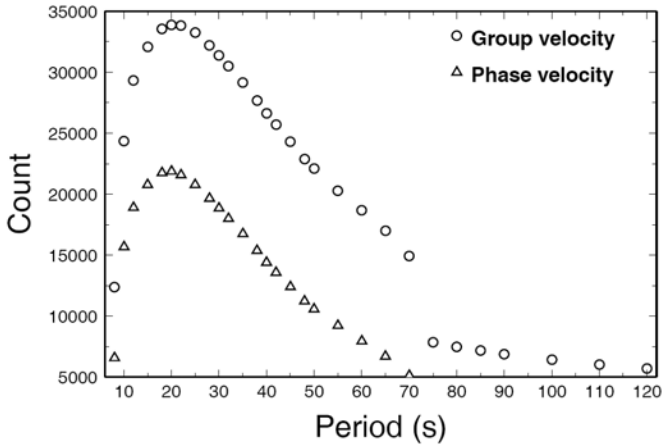

Figure 6. Distribution of Rayleigh group (open circles) and phase (open triangles) dispersion measurements for different periods. Note that the EGFs from both ambient noise correlation and earthquake data are included in Rayleigh group measurements up to 70 s. Only earthquake data are used for group dispersion measurements for periods longer than 70 s. To avoid initial phase ambiguity, earthquake data are not used in phase dispersion measurements.

Dispersion maps at different periods are constructed by minimizing the following equation:
$\min (\|\mathbf{Am}-\mathbf{r}\|^2+\lambda^2\|\mathbf{m}\|^2+\varphi^2\|\mathbf{Lm}\|^2)$.

The first term is a data misfit, in which **m** is the parameter vector, **A** is the coefficient matrix, and **r** is the vector of travel-time residuals. The second term is the model regularization with a damping parameter of non-zero real number λ. The third term is the smoothing constraint with non-zero real number φ. The smoothing operator **L** is the Laplacian operator (Lees and Crosson, 1989).

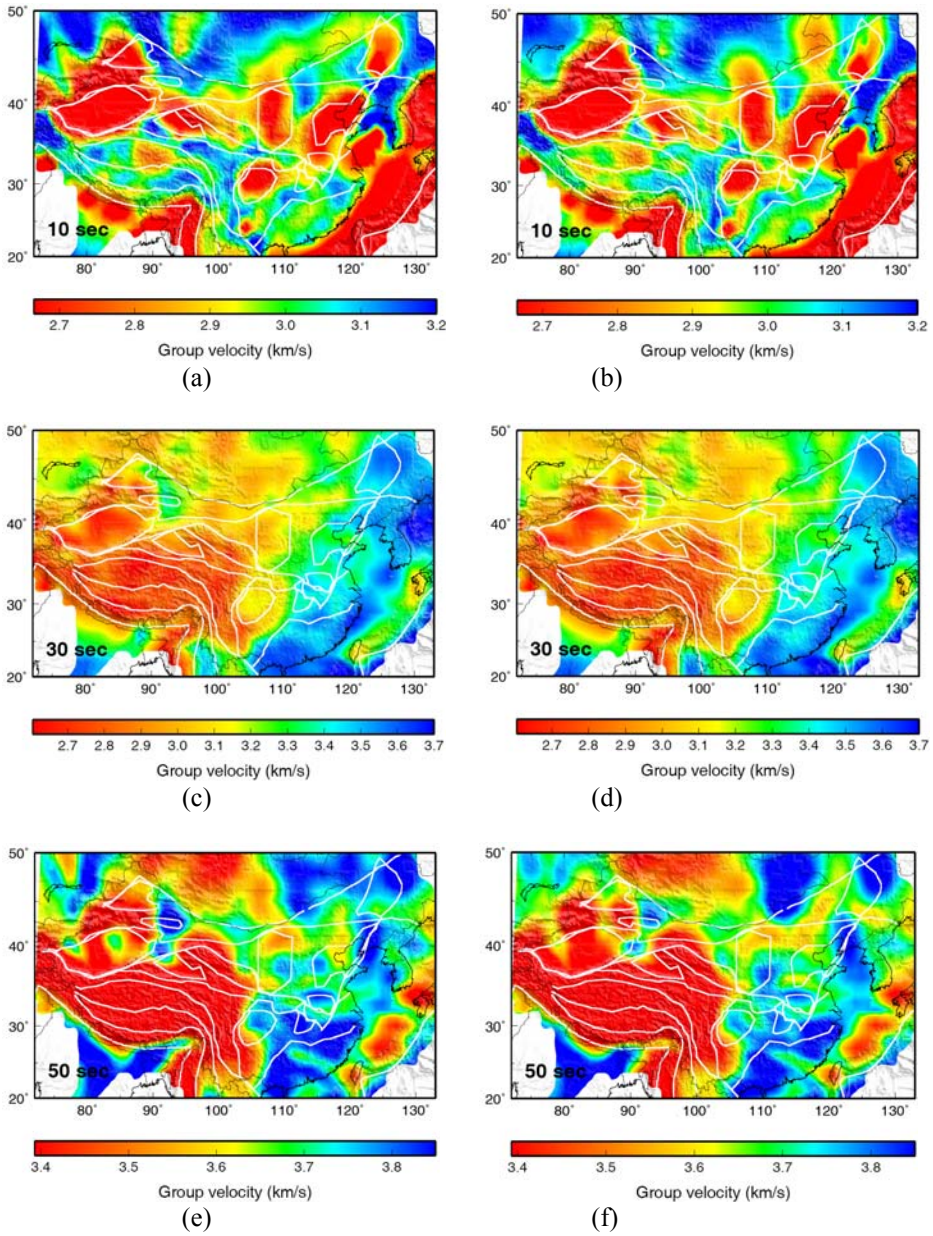

Figure 7. Group velocity maps at 10, 30, and 50 s, using EGFs and earthquake data (left) and earthquake data only (right). Results from two different datasets are generally compatible.

Examples of new dispersion maps are shown in Figure 7. Earthquake data account for about 50% of total group velocity measurements for periods from 8 to 70 s. We compare group velocity dispersion maps from earthquake data and the results using the whole dataset. The images are generally compatible (Figure 7). All large-scale major features are similar, e.g., low velocity in the sediment basin at short periods, a low-velocity zone throughout the Tibetan Plateau, and an eastern-western velocity contrast at mid periods, although there are differences in detailed structures.

CONCLUSIONS AND RECOMMENDATIONS

Our effort so far has focused on two areas. One is the joint inversion methods, which are done in two steps. The first step is to derive a joint P model from first-arriving Pg and Pn and secondary crustal direct P waves. The method has been demonstrated to be highly effective. The second step is to combine the P model and Pn station delays from the first step with receiver functions and Rayleigh-wave dispersion measurements to invert jointly for S wave structure and Moho depth. Another major effort is to increase dispersion measurements by including stations over a long period of time and by including traditional earthquake data. We increase the total number of dispersion measurements by four times. We have obtained a new set of dispersion maps. Maps from ambient noise data and earthquake data are highly compatible, both showing robust major features; thus, the combination greatly increases the resolution of the dispersion maps.

REFERENCES

Ammon, C. J., G. E. Randall, and G. Zandt (1990). On the nonuiqueness of receiver function inversions, *J. Geophys. Res.* 95: 15303–15318.

Benson, G. D., M. H. Ritzwoller, M. P. Barmin, A. L. Levshin, F. Lin, M. P. Moschetti, N. M. Shapiro, and Y. Yang (2007). Processing seismic ambient noise data to obtain reliable broad-band surface wave dispersion measurements, *Geophys. J. Int.* 169: 1239–1260.

Julia, J., C. J. Ammon, R. B. Herrmann, and A. M. Correig (2000). Joint inversion of receiver functions and surface-wave dispersion observations, *Geophys. J. Int*. 143: 99–112.

Lees, J. M. and R. S. Crosson (1989). Tomographic inversion for three-dimensional velocity structure at Mount St. Helens using earthquake data, *J. Geophys. Res*. 94: 5716–5728.

Levshin, A. L. and Ritzwoller, M. H. (2001). Automated detection, extraction, and measurement of regional surface waves, *Pure Appl. Geophys.* 158: 1531–1545.

Koketsu, K. and S. Sekine (1998). Pseudo-bending method for three-dimensional seismic ray tracing in a spherical Earth with discontinuities, *Geophys. J. Int*. 132: 339–346.

Ozalaybey, S., M. K. Savage, A. F. Sheehan, J. N. Louie, and J. N. Brune (1997). Shear-wave velocity structure in the northern basin and range province from the combined analysis of receiver functions and surface waves, *Bull. seism. Soc. Am*. 87: 183–189.

Song, X. D., Z. J. Xu, X. L. Sun, S. H. Zheng, Y.J . Yang, and M. H. Ritzwoller (2009). Surface wave dispersion measurements and tomography from ambient seismic noise correlation in China, in *Proceedings of the 2009 Monitoring Research Review: Ground-Based Nuclear Explosion Monitoring Technologies*, LA-UR-09-05276, Vol. 1, pp. 221–229.

Xu, Z. and X. D. Song (2009). Joint inversion for crustal and Pn velocities and Moho depth for eastern margin of Tibetan Plateau, *Tectonophys.* (in press).

Zheng, S. H., X. L. Sun, X. D. Song, Y. J. Yang, and M. H. Ritzwoller (2008). Surface wave tomography of China from ambient seismic noise correlation, *Geochem. Geophys. Geosyst*. 9: Q05020, doi:10.1029/2008GC001981, 2008.

Zhu, L. P. and H. Kanamori (2000). Moho depth variation in southern California from teleseismic receiver functions, *J. Geophys. Res*. 105: 2969–2980.